JOURNAL OF AIRCRAFT
Vol. 38, No. 5, September–October 2001

Algorithm for Prediction of Trailing Vortex Evolution

Robert E. Robins* and Donald P. Delisi†
Northwest Research Associates, Inc., Bellevue, Washington 98009-3027
and
George C. Greene‡
NASA Langley Research Center, Hampton, Virginia 23681-2199

We describe an algorithm that predicts the trajectories and circulation decay of aircraft trailing vortices. We first present the methodology used by the algorithm to simulate trailing vortex behavior, including 1) the descent of the vortices through a realistic atmosphere defined by crosswind, turbulence, and stratification profiles and 2) the interaction of the vortices with the ground. Examples are presented to demonstrate the algorithm's capability. We then describe a database approach for quantifying comparisons between algorithm predictions and measurements of wake vortex transport and decay. The use of databases to optimize the constant factor k in the term governing the effect of turbulence on vortex decay is reported, with the result that k appears to depend on the intensity of ambient turbulence. Using selected groupings of cases from the database, we have determined that vortices not interacting with the ground decay about a factor of two faster in high-intensity ambient turbulence than in low-intensity ambient turbulence. We also show that the circulation decay for vortices in the ground effect appears to be independent of the ambient turbulence level.

Nomenclature

b	=	vortex separation distance
b_0	=	initial vortex separation distance
k	=	circulation decay factor
q	=	turbulence velocity (q^2 = average over t^* of $u'u' + v'v' + w'w'$)
T	=	nondimensional time, t/T_0
T_0	=	time for vortices initially to descend a distance b_0, b_0/V_0
t	=	time after aircraft passage
t_{meas}	=	measured t for vortices to leave the aircraft vortex spacing system (AVOSS) corridor
t_{pred}	=	predicted t for vortices to leave the AVOSS corridor
t^*	=	averaging time for q
U	=	aircraft speed
u'	=	along runway wind fluctuation
V_0	=	initial vortex descent speed, $W/2\pi\rho U b_0^2$
v'	=	cross runway wind fluctuation
W	=	aircraft weight
w'	=	vertical wind fluctuation
x	=	along runway coordinate
y	=	cross runway coordinate
Z_a	=	altitude below which vortices are in near-ground effect phase
Z_b	=	altitude below which vortices are in in-ground effect phase
ZGEFAC	=	normalized Z_b, Z_b/b_0
ZIMFAC	=	normalized Z_a, Z_a/b_0
z	=	vertical coordinate
Γ	=	circulation
Γ_0	=	initial circulation
ΔT	=	absolute value of $(t_{\text{pred}} - t_{\text{meas}})/T_0$
$\Delta(\Gamma/\Gamma_0)$	=	normalized rms difference between predicted and measured circulation
ρ	=	atmospheric density

Received 2 March 2000; revision received 12 June 2001; accepted for publication 14 June 2001.

*Research Scientist, P.O. Box 3027. Senior Member AIAA.
†Senior Research Scientist, P.O. Box 3027. Senior Member AIAA.
‡Research Engineer; currently Acting Manager, Federal Aviation Administration, R&D Field Office, Mail Stop 250. Associate Fellow AIAA.

I. Introduction

FOR the past several years, NASA has been conducting research, under its Terminal Area Productivity Program, aimed at the development of an aircraft vortex spacing system (AVOSS).[1–3] The goal of AVOSS is to increase airport capacity while maintaining or increasing the present levels of aircraft safety. The approach of AVOSS is to use the observed and predicted weather state, algorithms for wake vortex transport and decay, wake vortex sensor data, and definitions of acceptable vortex strength to determine safe operating spacings between arriving and/or departing aircraft.

One important part of the AVOSS program is the development of an algorithm to predict how aircraft wake vortices evolve and decay in prevailing and expected weather conditions around an airport. The requirements of the algorithm are that it include the effects of important atmospheric parameters, such as wind, turbulence, and stratification, and that it be capable of seamlessly handling wake vortices out-of-ground effect (OGE), when the vortices are far from the ground, near-ground effect (NGE), when the trajectories of the vortices begin to be affected by the presence of the ground, and in-ground effect (IGE), when the vortices become close enough to the ground to cause the generation of secondary vorticity. Because of the real-time nature of AVOSS, another requirement is that the algorithm must almost instantly provide results for use by the system.

Many recent numerical studies of wake vortex evolution have incorporated sophisticated numerical approaches in their two-dimensional[4–7] or three-dimensional solutions.[8–11] However, these simulations take several tens of minutes or, in the worst cases, several tens of hours of supercomputer time to complete. Thus, it is not feasible at this time to use these models in a real-time airport control system such as AVOSS.

II. Methodology

We have developed an algorithm that meets the requirements of the AVOSS program, as outlined in the Introduction. The OGE phase of the algorithm is based on the model of Greene,[12] who assumes that the time rate of change of impulse per unit length of the vortex wake is due to viscous drag, buoyancy, and turbulent decay. We have enhanced Greene's approach to include vertical profiles of virtual potential temperature and turbulent kinetic energy (TKE) ($q^2/2$) for the representation of the buoyancy and turbulence effects, respectively, and a vertical profile of crosswind to include

horizontal transport of the vortex wake. These profiles are usually derived from meteorological observations such as those obtained in conjunction with recent AVOSS field campaigns at the Memphis (MEM) and Dallas–Fort Worth (DFW) airports.[13–15] Sarpkaya[16] and Sarpkaya et al.[17] have recently described a similar approach that excludes viscous drag and relies on vertical profiles of eddy dissipation rate instead of TKE to represent turbulent decay. [Note that the Sarpkaya et al. model was used in the successful demonstration of AVOSS at DFW International Airport during the week of 17 July 2000 (Ref. 17).]

Our representation of the NGE and IGE phases was inspired by previous studies reported by Liu,[18] Corjon and Poinsot,[19] and Corjon et al.[20] Liu[18] used a constrained secondary vortex to produce vortex rebound at the ground, although the boundary condition of zero vertical velocity at the ground was not satisfied. Corjon and Poinsot[19] and Corjon et al.[20] added ambient wind to Liu's[18] model for ground effect and added image vortices of the primary vortices only. Because image vortices of the secondary vortices were not used, zero vertical velocity at the ground was not satisfied.

Our algorithm extends these earlier studies by adding several new features. The following is an outline of how our algorithm treats the evolution of the vortex wake as it descends from the OGE phase, through the NGE phase, to the IGE phase:

1) Far above the ground, in the OGE phase, the algorithm uses the modified Greene[12] algorithm to compute the vortex trajectory and circulation decay (Fig. 1a). Using the equation $\Gamma_0 = W/\rho U b_0$, where ρ is atmospheric density at the generation height of the aircraft, the initial vortex strength Γ_0 is determined from the reported aircraft type (where the initial separation of the vortices, b_0, is $\pi/4$ times the wing span), aircraft weight W, and aircraft speed U.

2) When the vortex cores are at a height of $Z_a = b_0 \times$ ZIMFAC above the ground, the algorithm transfers the solution from the modified Greene algorithm to a pair of classic, inviscid point vortices and adds two image vortices below the ground (Fig. 1b). We call this region the NGE or image vortex phase. ZIMFAC is typically about 1.5.

3) In the NGE phase, the algorithm continues to use the same decay that occurred just before the vortices entered this phase.

4) When the vortex cores are at a height of $Z_b = b_0 \times$ ZGEFAC above the ground, the algorithm introduces ground-effect vortices (to represent generation of secondary vorticity) and their respective images. We call this region the IGE or ground-effect phase. Typically, ZGEFAC is about 0.6. After the first set of ground-effect vortices have rotated 180 deg around the primary vortices, a second set of ground-effect vortices, with images, is introduced into the flow (Fig. 1c). In Fig. 1 the plus symbols (dashed lines) indicate the location (trajectories) of the primary vortex cores. Curved arrows indicate the rotational directions of the the vortices. $Z_a = b_0 \times$ ZIMFAC and $Z_b = b_0 \times$ ZGEFAC define the image vortex region and the ground-effect region. The motivation for the second set of ground-effect vortices is to model the continual generation of secondary vorticity by the primary vortices.

Ground-effect vortices are initially introduced at a distance of $0.4b_0$ from and at an angle of 45 deg outboard of the primary vortices, and the initial circulation is 40% of each primary vortex. The circulation of the ground-effect vortices is a function of the rotation angle to allow for stronger secondary circulation near the ground. Typically, the maximum strength is at an angle of 45 deg, and the minimum strength occurs throughout the angle range 225–315 deg with secondary vortex strength varying linearly between these regions. Once introduced, the ground-effect vortices are unconstrained, and both lateral positions and vertical heights are determined by the interacting vortex dynamics.

5) The algorithm continues to let all vortices in the IGE phase decay at the same rate that occurred just before the primary vortices entered the NGE phase. The evolution is continued until a specified stop time. The various parameters defined earlier (1.5, 0.6, 180, 0.4, 45 deg, and 40%) have been determined from extensive comparisons with observations and results from large-eddy simulations.

The transitions between the OGE, NGE, and IGE phases are transparent to the user, and the vortices can start in any one of these three phases. (We note that, if the vortices start in the NGE or IGE regions, one time step is taken using the OGE algorithm to determine decay rate. This decay rate is then used in the remainder of the calculations.) A typical calculation using the algorithm for vortices lasting over 2 min takes less than 0.1 s to run on a Sun Ultra 1 workstation.

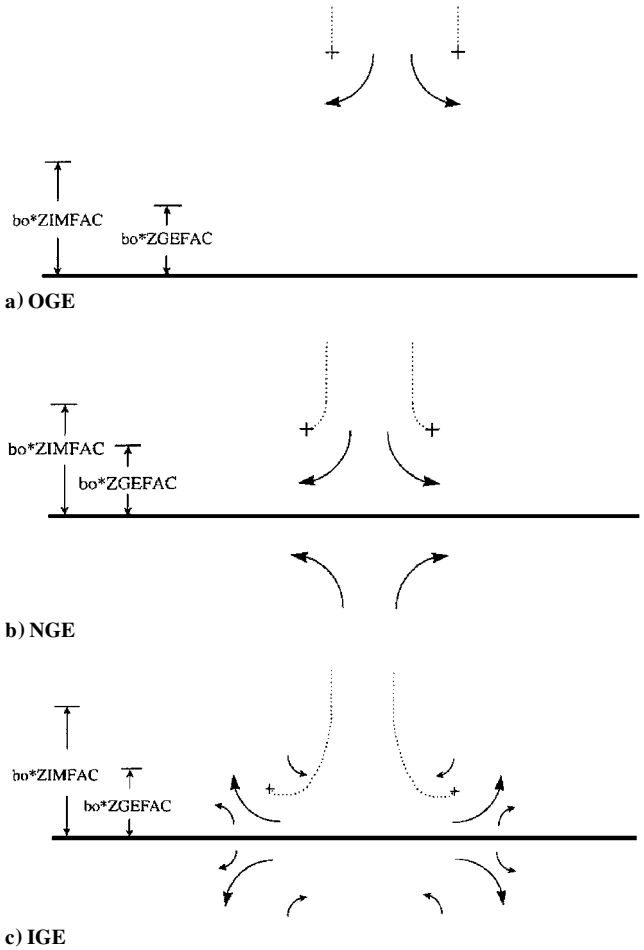

Fig. 1 Vortex geometry for algorithm phases.

III. Typical Results

Examples of typical algorithm results are as follows.

In Fig. 2a, we show data from MEM case 1254 on 16 August 1995. In this example, the lidar is located at the Armory, at a site approximately 2600 m to the south of the threshold of runway 36R and 66 m to the west of the runway centerline. The lidar was operated by Massachusetts Institute of Technology (MIT)/Lincoln Laboratories, under contract to NASA Langley Research Center.[13–15] The lidar is looking crosstrack, at a constant distance from the runway threshold. Figure 2a shows measurements of a Boeing-727/100 landing at 1719 hrs local time. The left plot in Fig. 2a shows altitude above the lidar van vs time after aircraft passage. The right plot shows altitude vs lateral position from the lidar van. Circles and × symbols represent lidar measurements of the port and starboard vortices, respectively. The horizontal and vertical lines associated with each data point are estimates of lateral and vertical position error of the lidar measurements.[13]

In both plots in Fig. 2a, the solid lines at altitudes of 79.8 and 123.9 m represent two corridor floors described by Hinton.[2] The solid rectangle at $t = 0$ in the left plot shows the reported beacon altitude (accurate to about ±50 ft) of the B-727. In the right plot, the solid horizontal line at 153.4 m is the glide slope altitude at the lidar position. The dashed, vertical line at 66 m in the right plot shows the runway centerline. The solid, vertical line at $Y = 134$ m is the east edge of the corridor described by Hinton.[2] In the right plot in Fig. 2a, the dotted, vertical line at $y = 97$ m shows the zero wind line; the thin, solid vertical line shows the reported wind profile, with 1 m/s being equivalent to $\Delta Y = 10$ m. This profile shows a

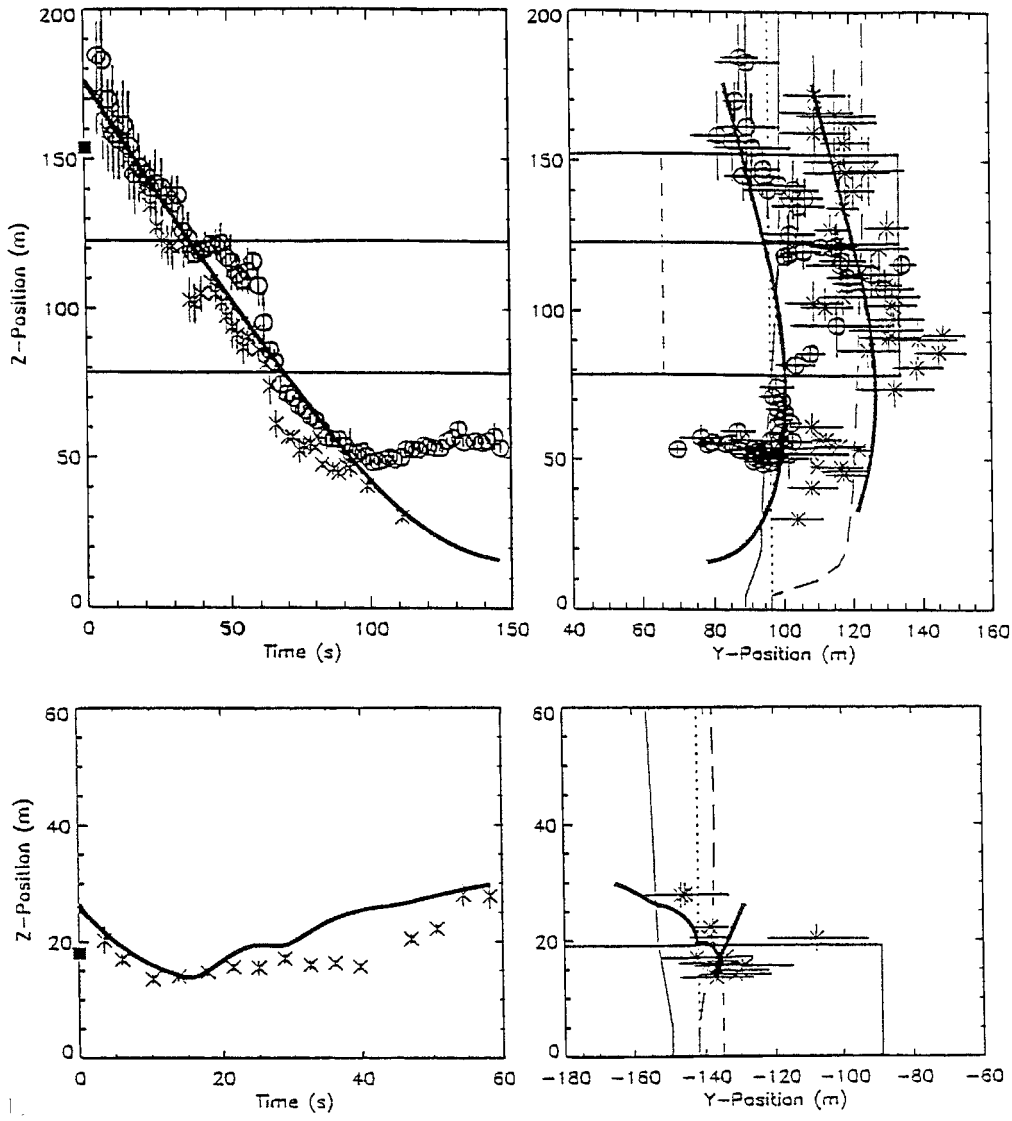

Fig. 2 Comparison of algorithm predictions and measurements for a) MEM case 1254 and b) MEM case 1480.

wind toward the west from 0 to ~75 m altitude and winds toward the east at higher altitudes. The long-dashed lines in the right hand plot of Fig. 2a is the potential temperature profile, with 1 deg K equivalent to $\Delta Y = 10$ m.

In the calculation, both the starting altitude and initial lateral position of the aircraft were inferred from the lidar measurements because this aircraft appeared to be located both above and to the east of the expected position. The algorithm result shows reasonable agreement with both the measured altitude vs time and the measured altitude vs lateral position for vortex evolution times less than around 100 s. For $t > 100$ s, the data show higher vortex altitudes than predicted by the algorithm. Because the ground in this lidar location was composed of high trees, we may be underestimating the effective ground height at the Armory in the algorithm, which could explain the differences for $t > 100$ s.

Note that the algorithm predicts the same vertical descent for both vortices, and so we would not expect the observed trajectory differences seen for the port and starboard vortices in the left plot in Fig. 2a to be predicted. Vertical crosswind gradients might be expected to cause asymmetry in the vortices' behavior,[21–24] but the algorithm does not currently include such effects. Also note that predictions are continued for only as long as there are observations to compare with. Thus, in this case, the port predictions last longer than the starboard predictions, which is why in the lateral position plot, the predicted port vortex trajectory descends closer to the ground than the predicted starboard vortex trajectory.

Figure 2b shows similar plots to Fig. 2a for MEM case 1480, an IGE case with a 727/100 landing at the threshold of runway 27 at 1754 hrs local time on 25 August 1995. Again, there is reasonable agreement between the algorithm results and the lidar measurements. In Fig. 2b, only the starboard vortex was observed, and so only the starboard predictions are plotted.

IV. Database Description

To quantify comparisons between algorithm results and observations of trailing vortex evolution, we have defined several numerical measures which are described subsequently. These quantities have been incorporated in a database, which also includes aircraft and environmental data. The database concept was originally suggested for use in the AVOSS program by Hinton and Proctor of the NASA Langley Research Center, and its format has been developed in conjunction with Hinton, Proctor, and Sarpkaya of the Naval Postgraduate School. The database will subsequently be referred to as the AVOSS prediction algorithm (APA) database.

The APA database has been constructed for two AVOSS observation periods, one at MEM in 1995 and a second at DFW in 1997. In each observation period, there were lidar measurements, made by MIT/Lincoln Laboratories, of aircraft wake vortices and concurrent meteorological observations.

The APA database consists of five groups of data elements. These groups are 1) identification information, 2) primary algorithm

evaluation data, 3) acquisition information, 4) environmental data, and 5) supplementary algorithm evaluation data. Each database record corresponds to the prediction and observation of the wake vortex evolution for the longest lived vortex from one aircraft (the other vortex is ignored).

Identification information includes the location, date, time, and duration of the lidar measurements for each aircraft passage. *Primary algorithm evaluation data* includes root-mean-square (rms) differences, over the duration of the observation, between predicted and observed vortex altitude, lateral position, and circulation. Also included are the predicted and measured times for circulation to decay below 150 m^2/s, and the predicted, t_{pred}, and measured, t_{meas}, time for a vortex to clear a defined corridor, the extent of which depends on the altitude of the glide slope. Definitions of corridor geometry are provided by Hinton.[2] In the work to be discussed, we use Hinton's floor 2 (which is higher in altitude than floor 1) as the bottom of the corridor.

Acquisition information includes the aircraft weight at the time of the observation, wing span, the initial altitude and circulation of the vortices, and the theoretical vortex descent rate (based on the aircraft weight, speed, and wing span). *Environmental data* include measures of various atmospheric parameters at the time of vortex generation. Some of these measures are TKE, eddy dissipation rate, Froude number, crosswind speed, crosswind vertical shear, crosswind vertical shear gradient, and Richardson number. These quantities are given either as a value at a sensor altitude or the vortex starting altitude, or as an average over the range of altitudes traversed by the vortex. *Supplementary algorithm evaluation data* include rms differences over 30-s time intervals between predicted and measured 1) altitude, 2) lateral position, and 3) circulation, and predicted and measured time for circulation to decay below 75 m^2/s.

The software for generating a database for a given set of trailing vortex cases consists of four modules: 1) the prediction algorithm, 2) a module for processing the environmental data and processing the first module's predictions of vortex trajectory and circulation decay, 3) a module for reading the lidar measurements of vortex location vs time and vortex velocity as a function of radius vs time, and deriving the observed aircraft vortex trajectories and circulations, and 4) a final module for evaluating the differences between the predictions and observations. The last module also maps the various database elements into the defined database format. Modules 2) and 3) are based on software developed by Dasey of MIT/Lincoln Laboratories for the purpose of processing and analyzing lidar observations of trailing wake vortices.

Applications of the APA database concept are evaluation of algorithm performance, optimization of algorithm performance, and study of environmental influences on algorithm behavior. In the following section, we show how the generation of database realizations has been used for algorithm optimization.

V. Algorithm Optimization

As an example of how we have used the APA database for algorithm optimization, we describe how we have identified the best value of the constant k, in the circulation decay term of the modified Greene model.[12] (Note that Greene's turbulent decay term is $d\Gamma/dt = -k\Gamma q/b$, where Γ is circulation, t is time, q is turbulence velocity, b is vortex separation distance, and k is a constant.[12]) In Greene's original model, $k = 0.82$. For this analysis, 268 cases from the MEM test and 247 cases from the DFW test have been used. For the MEM cases, databases were generated for values of $k = 0.00$, 0.10, 0.20, 0.30, 0.41, and 0.46. For the DFW cases, databases were generated for values of $k = 0.00$, 0.10, 0.20, 0.30, and 0.41. In addition, each database has been subdivided into high- and low-turbulence cases, depending on whether the 30-min average TKE at 40-m altitude (one of the environmental quantities stored in the database, denoted by TKE30) for a given case was less than or greater than 0.7 m^2/s^2. We used TKE30 to differentiate low from high turbulence because we wanted an atmospheric parameter that would quantify the presence of atmospheric structures that would affect both wake transport and wake decay. Figure 3 shows plots of TKE30 vs time of day for the MEM cases (Fig. 3a) and the DFW cases (Fig. 3b). We chose 0.7 m^2/s^2 as a reasonable level to distinguish between low- and high-turbulence cases.

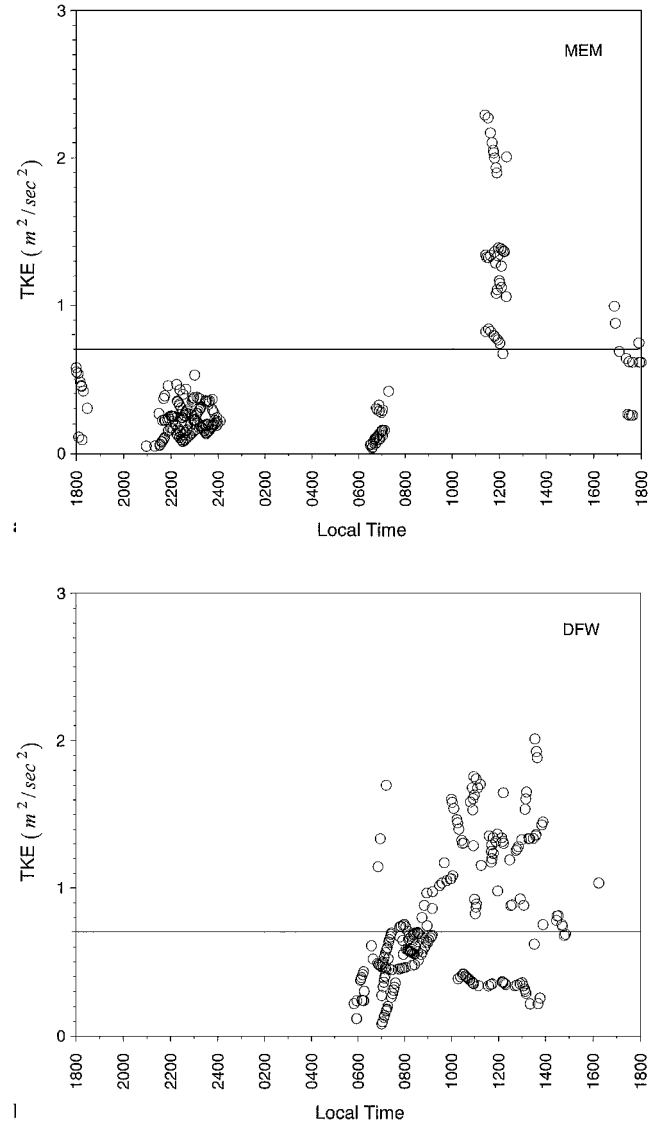

Fig. 3 Average TKE of 30 min vs local time for a) MEM and b) DFW.

We have focused on circulation decay and the normalized time difference between the predicted and measured time, ΔT, for a vortex to clear a defined corridor because these are important quantities to the AVOSS program. Here, the circulation decay $\Delta(\Gamma/\Gamma_0)$ is defined as the rms difference between predicted and measured circulation over the duration of the longest lived vortex from one aircraft passage, normalized by the initial circulation, and ΔT is the absolute value of $(t_{pred} - t_{meas})$ normalized by T_0, the time for the vortices initially to descend a distance equal to their separation. Here $T_0 = b_0/V_0$, where $V_0 = W/2\pi\rho U b_0^2$.

Figure 4 shows plots of how $\Delta(\Gamma/\Gamma_0)$ and ΔT vary with k for high- and low-turbulence cases. Figure 4 shows data for six groups of aircraft cases: MEM OGE (high and low TKE), MEM NGE (high and low TKE), and DFW NGE (high and low TKE). The number of cases used are MEM OGE low, $N = 152$; MEM OGE high, $N = 30$; MEM NGE low, $N = 23$; MEM NGE high, $N = 9$; DFW NGE low, $N = 156$; and DFW NGE high $N = 91$. In the plot, the solid symbols are for low turbulence (TKE30 < 0.7 m^2/s^2) and the open symbols are for high turbulence (TKE30 > 0.7 m^2/s^2). For each value of k for each aircraft case, we get one value of $\Delta(\Gamma/\Gamma_0)$. In Fig. 4a, we have chosen to plot the median value of each group for each value of k. The MEM OGE cases were obtained at the Armory location (glide slope altitude = 152 m) and the MEM NGE cases were obtained at the Tang location (glide

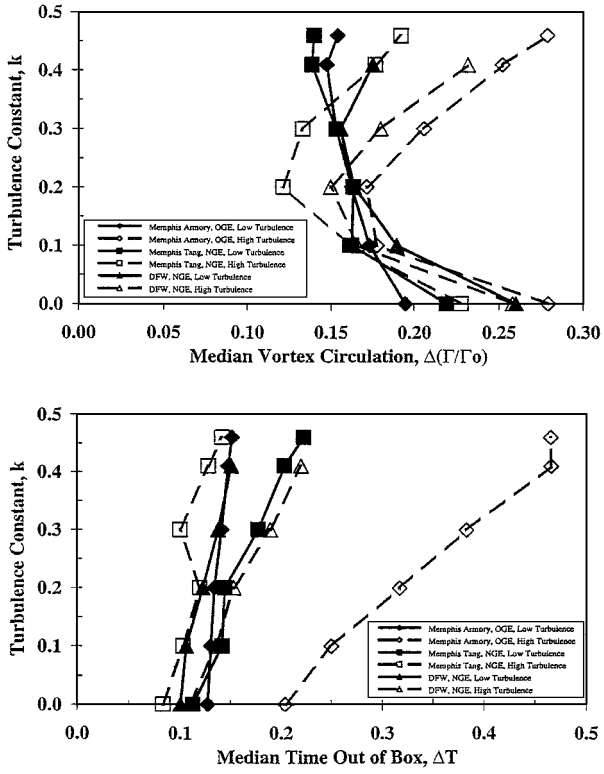

Fig. 4 Turbulence constant k vs a) median rms difference between predicted and measured normalized circulation and b) median absolute difference between predicted and measured normalized time for vortices to clear a defined corridor, for six groups of data identified in the legends.

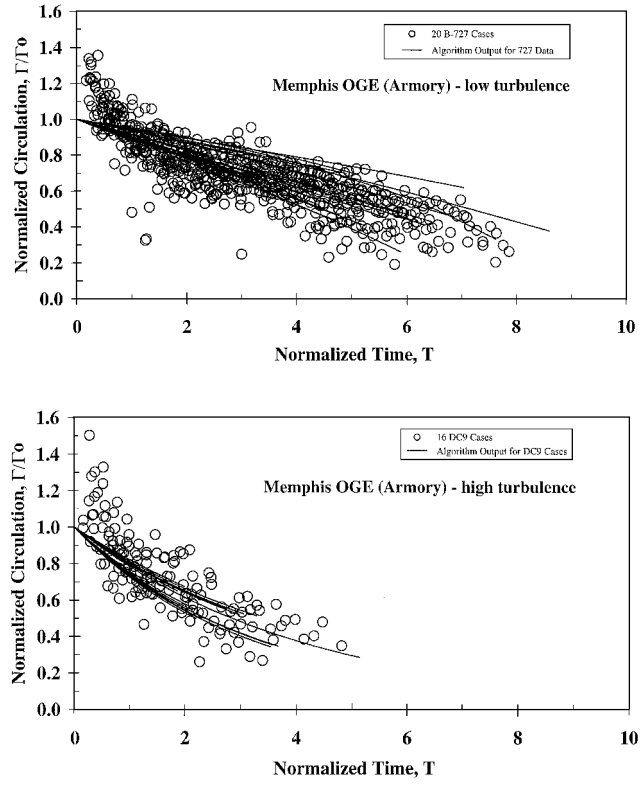

Fig. 5 Algorithm predictions and measurements of normalized circulation vs normalized time at the MEM Armory site for a) 20 B-727 low-turbulence cases and b) 16 DC9 high-turbulence cases.

slope altitude = 88 m). All DFW cases reported in this paper had the same approximate initial altitude (glide slope altitude = 84–93 m). We chose to look at the Armory data because there was a large amount of high-quality data gathered at that location, and we chose to look at Tang data because this was the only measurement location at MEM where the initial aircraft altitudes were approximately the same as those for the DFW cases.

Figure 4a shows that, for MEM, $k = 0.20$ gives the minimum value of $\Delta(\Gamma/\Gamma_0)$ for high turbulence for both the Armory and the Tang data and that $k = 0.41$ gives the minimum value for low turbulence at both locations. For DFW, $k = 0.20$ again gives the minimum value for high turbulence, whereas $k = 0.30$ gives the minimum value for low turbulence. To summarize, we note that the minimum value for k at both airports is 0.20 for high-turbulence values and is either 0.30 or 0.41 for low-turbulence values. We suspect the reason for the difference between minimum values for k at MEM and DFW for low-turbulence levels is that the turbulence levels were lower in the MEM grouping than in the DFW grouping. It, thus, appears that the optimum value of k in the modified Greene[12] model, to minimize $\Delta(\Gamma/\Gamma_0)$, depends on the atmospheric turbulence level.

In Fig. 4b, we see that $k = 0.00$ gives the minimum value for ΔT for all groups. This result is in sharp contrast to the results in Fig. 4a. We believe the reason for this difference is that, for the corridors being considered, the vortices leave a corridor before turbulence has had a chance to act on them. This point will be further discussed in the Comparisons section to follow.

The implication from the preceding results for the AVOSS program is that, when using the modified Greene[12] algorithm, k should be set to zero, when predicting time out of the corridor, and k should be set to a value depending on the ambient turbulence level when predicting circulation decay.

VI. Comparisons to Data

In this section, we show predictions of circulation decay for selected groupings of aircraft from MEM and DFW, using the optimum values of k [0.20 for low turbulence and 0.41 (MEM) or 0.30 (DFW) for high turbulence] derived from Fig. 4a. Figure 5a shows measurements and algorithm predictions from 20 Boeing-727 aircraft in low-turbulence conditions (TKE30 < 0.7 m^2/s^2) at the Armory OGE site at MEM. In this and the following plots, the symbols denote the circulations derived from the lidar measurements, the solid lines denote the predictions from the algorithm (one solid line for each aircraft measured), and the observed vortex circulations are calculated using a 3–10 m, two-sided average of the circulations measured by the MIT/Lincoln Laboratories lidar at 1-m increments from the vortex center.

We make the following observations from Fig. 5a. First, for all $T > 1$, the algorithm appears to predict the range of the measurements fairly well. Second, for these low-turbulence cases, the algorithm predictions are concave downward, with less decay at earlier times and increased decay at later times, which is consistent with the measurements for T greater than about 1.5. Finally, we note that at early times (for T less than about 0.5), the measured values of Γ/Γ_0 are greater than one. This overestimate of Γ/Γ_0 for early times most likely results from the inclusion of the vortices' descent velocity in the lidar measurement of the vortices' radial velocity. Effects from flap vortices may also play a role in these overestimates.

Figure 5b is similar to Fig. 5a, only for 16, high-turbulence (TKE30 > 0.7 m^2/s^2) DC9 aircraft at the Armory location at MEM. Again, we note that the predictions follow the data fairly well, with both the predictions and data showing at least a linear and perhaps a concave upward trend, with increased decay at earlier times and a slower rate of decay at later times. We note again the large values of Γ/Γ_0 for times T less than about 0.5.

Figure 6 shows similar data to Fig. 5 for NGE observations at the MEM Tang location. Because less data were obtained at the Tang location, there are fewer good cases to choose from. (By a good case, we mean one for which there is sufficient data that meaningful comparisons with predictions can be made.) Figure 6a shows data from five cases (two DC9, two Airbus 320, and one B727) in low turbulence, and Fig. 6b shows data from four cases (two DC9, one Airbus 320, and one B757) in high turbulence. Again, the algorithm predicts the trends of the measurements.

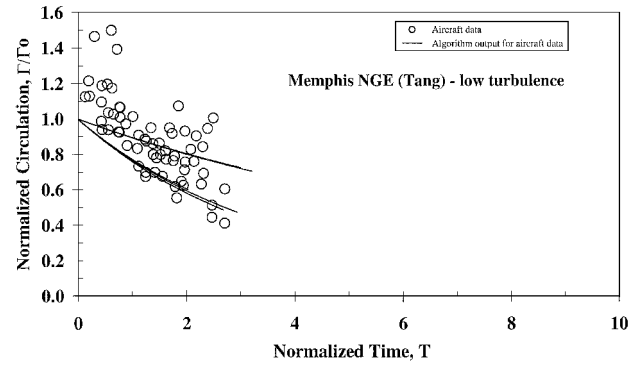

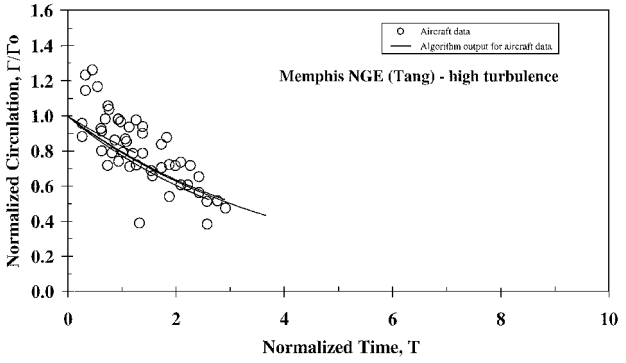

Fig. 6 Algorithm predictions and measurements of normalized circulation vs normalized time at the MEM Tang site for a) 5 low-turbulence cases and b) 4 high-turbulence cases.

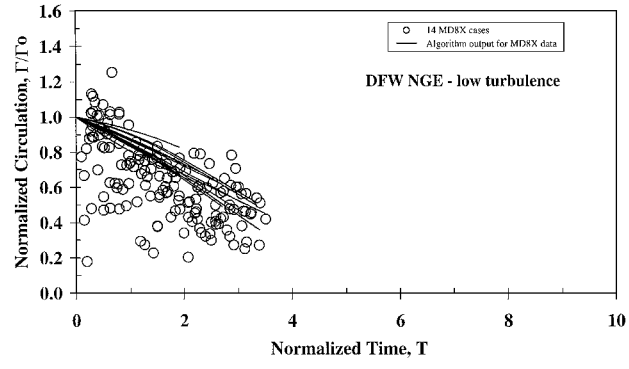

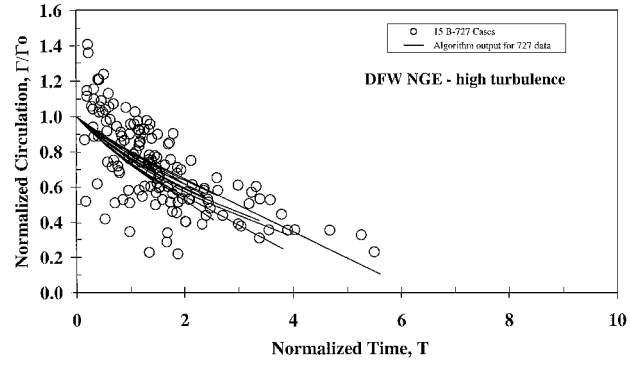

Fig. 7 Algorithm predictions and measurements of normalized circulation vs normalized time at DFW for a) 14 MD8X low-turbulence cases and b) 15 B-727 high-turbulence cases.

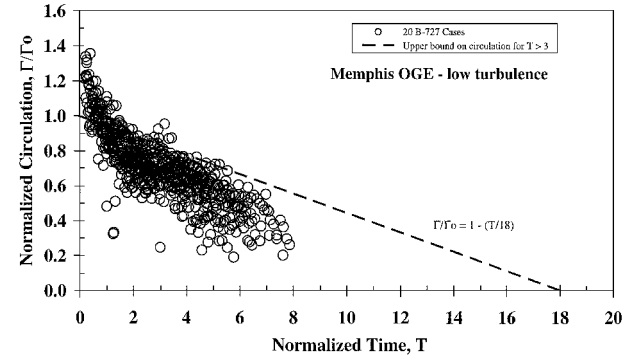

Fig. 8 Normalized circulation vs normalized time for 20 MEM B-727 low-turbulence cases.

Figure 7 shows similar NGE data at DFW, where the initial aircraft altitude was similar to that at Tang. Low-turbulence measurements and corresponding algorithm predictions for 14 MD8 series aircraft are shown in Fig. 7a. Here, the predictions are somewhat higher than many of the observations, although the observations have significantly more scatter at early times than observed at MEM. Figure 7b shows data from 15 Boeing-727 aircraft in high-turbulence conditions. We also note more scatter at early times in Figure 7b than at MEM (cf., Figs. 5b and 6b). In comparing Fig. 7b with Fig. 7a, we note that, although this may be due to only one or two of the runs, the data extend to longer times in the high-turbulence cases in Fig. 7b than in the low-turbulence cases in Fig. 7a. This is counter-intuitive because we would expect vortices in a low-turbulence environment to last longer than vortices in a high-turbulence environment. However, this result could be due to the proximity of the ground because we expect the vortices to be affected by the ground starting around $T \sim 2$.

If we visually overlay all of the measurements in Figs. 5–7, we see that most of the measurements overlap for nondimensional times less than about 1.5. This indicates that it takes a nondimensional time of around 1.5 for ambient turbulence to affect vortex circulation. Because T_0 for a landing, commercial aircraft is (dimensionally) typically around 15–20 s, this indicates that, for the first 20–30 s, the vortices are insensitive to the effects of ambient turbulence.

We also note that, for the corridors considered here, the nominal time for the vortices to exit the AVOSS box is around 30 s, or a T of ~1.5. Because during this time the vortices are insensitive to the intensity of the ambient turbulence, it follows that the time for the vortices to exit the box should not be a function of the ambient turbulence. This reasoning adds support to the result shown in Fig. 4b that $k = 0.00$ is the optimum value in computing ΔT, the time for the vortices to clear the corridor.

To clarify the difference between low and high ambient turbulence conditions, we next look at placing bounds on circulation values for the data shown earlier. Figure 8 is a replot of Fig. 5a where the dashed line is $\Gamma/\Gamma_0 = 1-(T/18)$. We note that all of the measured values of circulation are below this line for T greater than about 3. In contrast, Fig. 9 is a replot of Fig. 5b, where the dashed line, which bounds the data for times T greater than about 2, is $\Gamma/\Gamma_0 = 1-(T/9)$. For MEM Armory data, then, we see by comparing the two dashed lines that the effect of high ambient turbulence is to increase the vortex decay by a factor of about two.

In Fig. 10, we plot all of the circulation measurements from Figs. 6 and 7. These data all have similar starting altitudes. Also plotted in Fig. 10 are the bounding lines $\Gamma/\Gamma_0 = 1-(T/18)$ and $1-(T/9)$ from Figs. 8 and 9. Although the data are not conclusive, there is an indication that the line $\Gamma/\Gamma_0 = 1-(T/9)$ may be the better bound to the data. We note that we have plotted both low- and high-turbulence cases in Fig. 10. Thus, if this result holds up to additional scrutiny, it would indicate that when vortices interact with the ground, their decay rate is independent of the ambient turbulence intensity. This idea was first proposed by Burnham (private communication, 1998).

Finally, we note that laboratory experiments and numerical simulations have long suggested that the slowest decaying and longest lasting vortices should occur OGE in a low turbulence, weakly

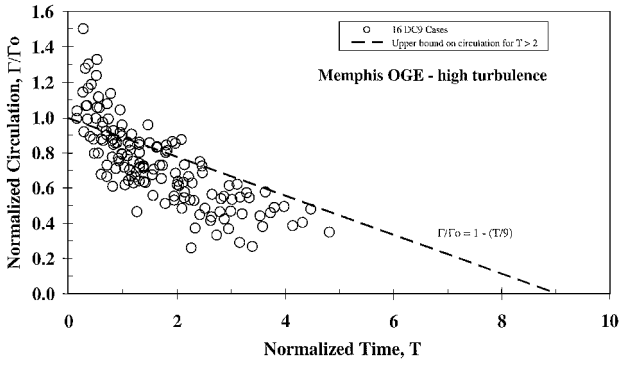

Fig. 9 Normalized circulation vs normalized time for 16 MEM DC9 high-turbulence cases.

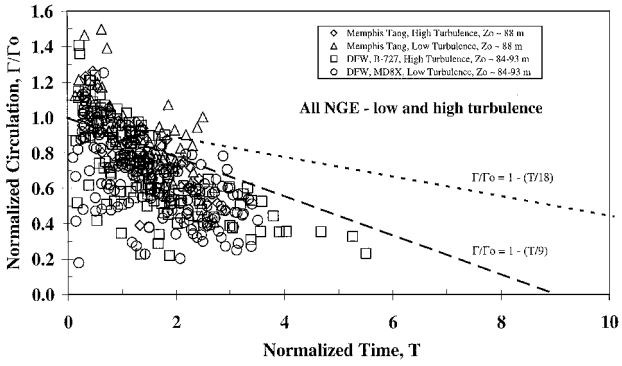

Fig. 10 Normalized circulation vs normalized time for 5 MEM Tang low-turbulence cases, 4 MEM Tang high-turbulence cases, 14 DFW MD8X low-turbulence cases, and 15 DFW B-727 high-turbulence cases.

stratified environment.[8,25] The data from the MEM Armory location in low turbulence (Figs. 5a and 8) support that hypothesis.

VII. Conclusions

We have described an engineering model of trailing vortex evolution that represents circulation decay due to turbulence away from the ground by a term containing the product of a constant k and the ambient turbulence velocity. We have used a database containing comparisons between predictions and observations of vortex evolution for 515 cases from MEM and DFW international airports to determine the value of k, with the result that $k = 0.20$ for low-turbulence cases and either 0.41 (MEM) or 0.30 (DFW) for high-turbulence cases.

From an examination of circulation decay observations for selected groupings of the 515 cases referred to, we have arrived at the following results:

1) Vortices not interacting with the ground (OGE and NGE), decay faster in high turbulence, but are insensitive to the turbulence for the first 20–30 s of their evolution.

2) For OGE cases, the effect of high-turbulence levels is to increase the circulation decay rate by about a factor of two.

3) NGE results suggest that circulation decay for vortices IGE is independent of the ambient turbulence level.

Acknowledgments

We gratefully acknowledge the support and encouragement of D. A. Hinton of NASA Langley Research Center. We also wish to acknowledge useful discussions with F. Proctor of NASA Langley Research Center, T. Sarpkaya of the Naval Postgraduate School, and T. Dasey of Massachusetts Institute of Technology Lincoln Laboratories.

References

[1]Hinton, D. A., "Aircraft Vortex Spacing System (AVOSS) Conceptual Design," NASA TM-110184, 1995.

[2]Hinton, D. A., "An Aircraft Vortex Spacing System (AVOSS) For Dynamical Wake Vortex Spacing Criteria," *Proceedings of the AGARD Symposium on The Characterisation and Modification of Wakes from Lifting Vehicles in Fluids*, CP-584, AGARD, 1996, pp. 23-1–23-12.

[3]Hinton, D. A., Charnock, J. K., Bagwell, D. R., and Grigsby, D., "NASA Aircraft Vortex Spacing System Development Status," AIAA Paper 99-0753, Jan. 1999.

[4]Proctor, F. H., "Numerical Simulation of Wake Vortices Measured During the Idaho Falls and Memphis Field Programs," AIAA Paper 96-2496, June 1996.

[5]Proctor, F. H., Hinton, D. A., Han, J., Schowalter, D. G., and Lin, Y.-L., "Two-Dimensional Wake Vortex Simulations in the Atmosphere: Preliminary Sensitivity Studies," AIAA Paper 97-0056, Jan. 1997.

[6]Spalart, P. R., "On the Motion of Laminar Wing Wakes in a Stratified Fluid," *Journal of Fluid Mechanics*, Vol. 327, 1996, pp. 139–160.

[7]Zheng, Z. C., and Ash, R. L., "Study of Aircraft Wake Vortex Behavior Near the Ground," *AIAA Journal*, Vol. 34, No. 3, 1996, pp. 580–589.

[8]Robins, R. E., and Delisi, D. P., "Numerical Simulations of Three-Dimensional Trailing Vortex Evolution in Stratified Fluid," *AIAA Journal*, Vol. 36, No. 6, 1998, pp. 981–985.

[9]Robins, R. E., and Delisi, D. P., "Numerical Simulations of Three-Dimensional Trailing Vortex Evolution," *AIAA Journal*, Vol. 35, No. 9, 1997, pp. 1552–1555.

[10]Proctor, F. H., "The NASA-Langley Wake Vortex Modelling Effort in Support of an Operational Aircraft Spacing System," AIAA Paper 98-0589, Jan. 1998.

[11]Corjon, A., Darracq, D., Venzac, P., and Bougeault, P., "Three-Dimensional Large Eddy Simulation of Wake Vortices. Comparison with Field Measurements," AIAA Paper 97-2309, June 1997.

[12]Greene, G. C., "An Approximate Model of Vortex Decay in the Atmosphere," *Journal of Aircraft*, Vol. 23, No. 7, 1986, pp. 566–573.

[13]Campbell, S. D., Dasey, T. J., Freehart, R. E., Heinrichs, R. M., Matthews, M. P., Perras, G. H., and Rowe, G. S., "Wake Vortex Field Measurement Program at Memphis, TN, Data Guide," Project Rept. NASA/L-2, Lincoln Lab., Massachusetts Inst. of Technology, Cambridge, MA, Jan. 1997.

[14]Dasey, T. J., Cole, R. E., Heinrichs, R. M., Matthews, M. P., and Perras, G. H., "Aircraft Vortex Spacing System (AVOSS) Initial 1997 System Deployment at Dallas/Ft. Worth (DFW) Airport," Project Rept. NASA/L-3, Lincoln Lab., Massachusetts Inst. of Technology, Cambridge, MA, July 1998.

[15]Joseph, R. M., Dasey, T. J., and Heinrichs, R. M., "Vortex and Meteorological Measurements at Dallas/Ft. Worth Airport," AIAA Paper 99-0760, Jan. 1999.

[16]Sarpkaya, T., "New Model for Vortex Decay in the Atmosphere," *Journal of Aircraft*, Vol. 37, No. 1, 2000, pp. 53–61.

[17]Sarpkaya, T., Robins, R. E., and Delisi, D. P., "Wake-Vortex Eddy-Dissipation Model Predictions Compared with Observations," *AIAA Journal*, Vol. 38, No. 4, 2001, pp. 687–692.

[18]Liu, H.-T., "Tow-Tank Simulation of Vortex Wake Dynamics," *Proceedings of the Aircraft Wake Vortices Conference*, edited by J. N. Hallock, Federal Aviation Administration, FAA Rept. SD-92, Oct. 1991.

[19]Corjon, A., and Poinsot, T., "Vortex Model to Define Safe Aircraft Separation Distances," *Journal of Aircraft*, Vol. 33, No. 3, 1996, pp. 547–553.

[20]Corjon, A., Zheng, Z. C., and Greene, G. C., "Model of the Behavior of Aircraft Wake Vortices Experiencing Crosswind Near the Ground," AIAA Paper 96-2516, June 1996.

[21]Burnham, D. C., "Effect of Ground Wind Shear on Aircraft Trailing Vortices," *AIAA Journal*, Vol. 10, No. 8, 1972, pp. 1114, 1115.

[22]Liu, C. H., and Ting, L., "Interaction of Decaying Trailing Vortices in Spanwise Shear Flow," *Computers and Fluids*, Vol. 15, No. 1, 1987, pp. 77–92.

[23]Proctor, F. H., Hinton, D. A., Han, J., Schowalter, D. G., and Lin, Y.-L., "Two Dimensional Wake Vortex Simulations in the Atmosphere: Preliminary Sensitivity Studies," AIAA Paper 97-0056, Jan. 1977.

[24]Proctor, F. H., "The NASA-Langley Wake Vortex Modelling Effort in Support of an Operational Aircraft Spacing System," AIAA Paper 98-0589, Jan. 1998 (invited paper).

[25]Sarpkaya, T., and Daly, J. J., "Effect of Ambient Turbulence on Trailing Vortices," *Journal of Aircraft*, Vol. 24, No. 6, 1987, pp. 399–404.